Eur. Phys. J. C 11, 587–598 (1999)
Digital Object Identifier (DOI) 10.1007/s100529900206

THE EUROPEAN PHYSICAL JOURNAL C

A study of B_s^0 meson oscillation using hadronic Z^0 decays containing leptons

The OPAL Collaboration

G. Abbiendi[2], K. Ackerstaff[8], G. Alexander[23], J. Allison[16], N. Altekamp[5], K.J. Anderson[9], S. Anderson[12], S. Arcelli[17], S. Asai[24], S.F. Ashby[1], D. Axen[29], G. Azuelos[18,a], A.H. Ball[8], E. Barberio[8], R.J. Barlow[16], J.R. Batley[5], S. Baumann[3], J. Bechtluft[14], T. Behnke[27], K.W. Bell[20], G. Bella[23], A. Bellerive[9], S. Bentvelsen[8], S. Bethke[14], S. Betts[15], O. Biebel[14], A. Biguzzi[5], I.J. Bloodworth[1], P. Bock[11], J. Böhme[14], D. Bonacorsi[2], M. Boutemeur[33], S. Braibant[8], P. Bright-Thomas[1], L. Brigliadori[2], R.M. Brown[20], H.J. Burckhart[8], P. Capiluppi[2], R.K. Carnegie[6], A.A. Carter[13], J.R. Carter[5], C.Y. Chang[17], D.G. Charlton[1,b], D. Chrisman[4], C. Ciocca[2], P.E.L. Clarke[15], E. Clay[15], I. Cohen[23], J.E. Conboy[15], O.C. Cooke[8], J. Couchman[15], C. Couyoumtzelis[13], R.L. Coxe[9], M. Cuffiani[2], S. Dado[22], G.M. Dallavalle[2], R. Davis[30], S. De Jong[12], A. de Roeck[8], P. Dervan[15], K. Desch[27], B. Dienes[32,h], M.S. Dixit[7], J. Dubbert[33], E. Duchovni[26], G. Duckeck[33], I.P. Duerdoth[16], P.G. Estabrooks[6], E. Etzion[23], F. Fabbri[2], A. Fanfani[2], M. Fanti[2], A.A. Faust[30], L. Feld[10], F. Fiedler[27], M. Fierro[2], I. Fleck[10], A. Frey[8], A. Fürtjes[8], D.I. Futyan[16], P. Gagnon[7], J.W. Gary[4], G. Gaycken[27], C. Geich-Gimbel[3], G. Giacomelli[2], P. Giacomelli[2], V. Gibson[5], W.R. Gibson[13], D.M. Gingrich[30,a], D. Glenzinski[9], J. Goldberg[22], W. Gorn[4], C. Grandi[2], K. Graham[28], E. Gross[26], J. Grunhaus[23], M. Gruwé[27], C. Hajdu[31] G.G. Hanson[12], M. Hansroul[8], M. Hapke[13], K. Harder[27], A. Harel[22], C.K. Hargrove[7], M. Harin-Dirac[4], M. Hauschild[8], C.M. Hawkes[1], R. Hawkings[27], R.J. Hemingway[6], G. Herten[10], R.D. Heuer[27], M.D. Hildreth[8], J.C. Hill[5], P.R. Hobson[25], A. Hocker[9], K. Hoffman[8], R.J. Homer[1], A.K. Honma[28,a], D. Horváth[31,c], K.R. Hossain[30], R. Howard[29], P. Hüntemeyer[27], P. Igo-Kemenes[11], D.C. Imrie[25], K. Ishii[24], F.R. Jacob[20], A. Jawahery[17], H. Jeremie[18], M. Jimack[1], C.R. Jones[5], P. Jovanovic[1], T.R. Junk[6], N. Kanaya[24], J. Kanzaki[24], D. Karlen[6], V. Kartvelishvili[16], K. Kawagoe[24], T. Kawamoto[24], P.I. Kayal[30], R.K. Keeler[28], R.G. Kellogg[17], B.W. Kennedy[20], D.H. Kim[19], A. Klier[26], T. Kobayashi[24], M. Kobel[3,d], T.P. Kokott[3], M. Kolrep[10], S. Komamiya[24], R.V. Kowalewski[28], T. Kress[4], P. Krieger[6], J. von Krogh[11], T. Kuhl[3], P. Kyberd[13], G.D. Lafferty[16], H. Landsman[22], D. Lanske[14], J. Lauber[15], I. Lawson[28], J.G. Layter[4], D. Lellouch[26], J. Letts[12], L. Levinson[26], R. Liebisch[11], B. List[8], C. Littlewood[5], A.W. Lloyd[1], S.L. Lloyd[13], F.K. Loebinger[16], G.D. Long[28], M.J. Losty[7], J. Lu[29], J. Ludwig[10], D. Liu[12], A. Macchiolo[18], A. Macpherson[30], W. Mader[3], M. Mannelli[8], S. Marcellini[2], A.J. Martin[13], J.P. Martin[18], G. Martinez[17], T. Mashimo[24], P. Mättig[26], W.J. McDonald[30], J. McKenna[29], E.A. Mckigney[15], T.J. McMahon[1], R.A. McPherson[28], F. Meijers[8], P. Mendez-Lorenzo[33], F.S. Merritt[9], H. Mes[7], A. Michelini[2], S. Mihara[24], G. Mikenberg[26], D.J. Miller[15], W. Mohr[10], A. Montanari[2], T. Mori[24], K. Nagai[8], I. Nakamura[24], H.A. Neal[12,g], R. Nisius[8], S.W. O'Neale[1], F.G. Oakham[7], F. Odorici[2], H.O. Ogren[12], A. Okpara[11], M.J. Oreglia[9], S. Orito[24], G. Pásztor[31], J.R. Pater[16], G.N. Patrick[20], J. Patt[10], R. Perez-Ochoa[8], S. Petzold[27], P. Pfeifenschneider[14], J.E. Pilcher[9], J. Pinfold[30], D.E. Plane[8], P. Poffenberger[28], B. Poli[2], J. Polok[8], M. Przybycień[8,e], A. Quadt[8], C. Rembser[8], H. Rick[8], S. Robertson[28], S.A. Robins[22], N. Rodning[30], J.M. Roney[28], S. Rosati[3], K. Roscoe[16], A.M. Rossi[2], Y. Rozen[22], K. Runge[10], O. Runolfsson[8], D.R. Rust[12], K. Sachs[10], T. Saeki[24], O. Sahr[33], W.M. Sang[25], E.K.G. Sarkisyan[23], C. Sbarra[29], A.D. Schaile[33], O. Schaile[33], P. Scharff-Hansen[8], J. Schieck[11], S. Schmitt[11], A. Schöning[8], M. Schröder[8], M. Schumacher[3], C. Schwick[8], W.G. Scott[20], R. Seuster[14], T.G. Shears[8], B.C. Shen[4], C.H. Shepherd-Themistocleous[5], P. Sherwood[15], G.P. Siroli[2], A. Sittler[27], A. Skuja[17], A.M. Smith[8], G.A. Snow[17], R. Sobie[28], S. Söldner-Rembold[10,f], S. Spagnolo[20], M. Sproston[20], A. Stahl[3], K. Stephens[16], J. Steuerer[27], K. Stoll[10], D. Strom[19], R. Ströhmer[33], B. Surrow[8], S.D. Talbot[1], P. Taras[18], S. Tarem[22], R. Teuscher[9], M. Thiergen[10], J. Thomas[15], M.A. Thomson[8], E. Torrence[8], S. Towers[6], I. Trigger[18], Z. Trócsányi[32], E. Tsur[23], M.F. Turner-Watson[1], I. Ueda[24], R. Van Kooten[12], P. Vannerem[10], M. Verzocchi[8], H. Voss[3], F. Wäckerle[10], A. Wagner[27], C.P. Ward[5], D.R. Ward[5], P.M. Watkins[1], A.T. Watson[1], N.K. Watson[1], P.S. Wells[8], N. Wermes[3], D. Wetterling[11] J.S. White[6], G.W. Wilson[16], J.A. Wilson[1], T.R. Wyatt[16], S. Yamashita[24], V. Zacek[18], D. Zer-Zion[8]

[1] School of Physics and Astronomy, University of Birmingham, Birmingham B15 2TT, UK
[2] Dipartimento di Fisica dell' Università di Bologna and INFN, 40126 Bologna, Italy
[3] Physikalisches Institut, Universität Bonn, 53115 Bonn, Germany
[4] Department of Physics, University of California, Riverside CA 92521, USA
[5] Cavendish Laboratory, Cambridge CB3 0HE, UK
[6] Ottawa-Carleton Institute for Physics, Department of Physics, Carleton University, Ottawa, Ontario K1S 5B6, Canada
[7] Centre for Research in Particle Physics, Carleton University, Ottawa, Ontario K1S 5B6, Canada
[8] CERN, European Organisation for Particle Physics, 1211 Geneva 23, Switzerland

[9] Enrico Fermi Institute and Department of Physics, University of Chicago, Chicago IL 60637, USA
[10] Fakultät für Physik, Albert Ludwigs Universität, 79104 Freiburg, Germany
[11] Physikalisches Institut, Universität Heidelberg, 69120 Heidelberg, Germany
[12] Indiana University, Department of Physics, Swain Hall West 117, Bloomington IN 47405, USA
[13] Queen Mary and Westfield College, University of London, London E1 4NS, UK
[14] Technische Hochschule Aachen, III Physikalisches Institut, Sommerfeldstrasse 26-28, 52056 Aachen, Germany
[15] University College London, London WC1E 6BT, UK
[16] Department of Physics, Schuster Laboratory, The University, Manchester M13 9PL, UK
[17] Department of Physics, University of Maryland, College Park, MD 20742, USA
[18] Laboratoire de Physique Nucléaire, Université de Montréal, Montréal, Quebec H3C 3J7, Canada
[19] University of Oregon, Department of Physics, Eugene OR 97403, USA
[20] CLRC Rutherford Appleton Laboratory, Chilton, Didcot, Oxfordshire OX11 0QX, UK
[22] Department of Physics, Technion-Israel Institute of Technology, Haifa 32000, Israel
[23] Department of Physics and Astronomy, Tel Aviv University, Tel Aviv 69978, Israel
[24] International Centre for Elementary Particle Physics and Department of Physics, University of Tokyo, Tokyo 113-0033, and Kobe University, Kobe 657-8501, Japan
[25] Institute of Physical and Environmental Sciences, Brunel University, Uxbridge, Middlesex UB8 3PH, UK
[26] Particle Physics Department, Weizmann Institute of Science, Rehovot 76100, Israel
[27] Universität Hamburg/DESY, II Institut für Experimental Physik, Notkestrasse 85, 22607 Hamburg, Germany
[28] University of Victoria, Department of Physics, P O Box 3055, Victoria BC V8W 3P6, Canada
[29] University of British Columbia, Department of Physics, Vancouver BC V6T 1Z1, Canada
[30] University of Alberta, Department of Physics, Edmonton AB T6G 2J1, Canada
[31] Research Institute for Particle and Nuclear Physics, 1525 Budapest, P O Box 49, Hungary
[32] Institute of Nuclear Research, 4001 Debrecen, P O Box 51, Hungary
[33] Ludwigs-Maximilians-Universität München, Sektion Physik, Am Coulombwall 1, 85748 Garching, Germany

Received: 21 June 1999 / Published online: 28 September 1999

Abstract. A sample of Z^0 decays containing b-flavoured hadrons is tagged using leptons, and events having precise proper time measurements are selected. These events are used to study B_s^0 oscillations. The flavour (b or $\bar{b}$) at decay is determined from the lepton charge while the flavour at production is determined from jet charge or the charge of a second lepton, where available. The experiment was not able to resolve the oscillatory behaviour, and we deduce that the B_s^0 oscillation frequency $\Delta m_s > 5.2$ ps^{-1} at the 95% confidence level.

1 Introduction

The phenomenon of $B - \bar{B}$ mixing is now well established. In the case of the B_d^0 system, the mass difference, Δm_d, between the two B_d^0 mass eigenstates has been measured rather precisely [1]. This mass difference gives the oscillation frequency between B_d^0 and $\bar{B}_d^0$. Although these measurements can be used to gain information on the CKM matrix element V_{td}, this is hampered by large theoretical uncertainties on both the meson decay constant, $f_{B_d^0}$, and the QCD bag model vacuum insertion parameter, $B_{B_d^0}$ [2]. This difficulty may be overcome if Δm_s, the B_s^0 oscillation frequency, is also measured. In this case, the CKM information can be extracted via the relation

$$\frac{\Delta m_s}{\Delta m_d} = \frac{m_{B_s^0}}{m_{B_d^0}} \cdot \frac{|V_{ts}|^2}{|V_{td}|^2} \cdot \frac{f_{B_s^0}^2 B_{B_s^0}}{f_{B_d^0}^2 B_{B_d^0}} , \qquad (1)$$

where $m_{B_s^0}$ and $m_{B_d^0}$ are the B_s^0 and B_d^0 masses, as the ratio of decay constants for B_d^0 and B_s^0 mesons is much better known than the absolute values [2,3]. Information on $|V_{td}|$ could then be extracted by inserting $|V_{ts}|$, which is relatively well known [1].

The most restrictive of the published limits [4–7] indicates that $\Delta m_s > 9.6$ ps^{-1}[6], while the previous best limit from OPAL [4] gives $\Delta m_s > 3.1$ ps^{-1}.

A study of B_s^0 oscillation is presented in this paper, using lepton charge to tag the flavour of the B_s^0 at decay and a jet charge technique (Sect. 3), or opposite-jet leptons where available, to tag the B_s^0 flavour at production. The analysis studies the oscillation as a function of the proper decay-time reconstructed using secondary vertices (Sect. 2), using a purity in semileptonic b-decays which is evaluated event-by-event (Sect. 4). Note that the analysis is sensitive to both B_s^0 and B_d^0 oscillation, but is optimised for the study of B_s^0 oscillation; the parameters describing the B_d^0 system are input from previous measurements.

The analysis technique is similar to that presented in previous papers [4,5], but includes more data (from 1995), takes advantage of three-dimensional vertexing, and fea-

[a] and at TRIUMF, Vancouver, Canada V6T 2A3
[b] and Royal Society University Research Fellow
[c] and Institute of Nuclear Research, Debrecen, Hungary
[d] on leave of absence from the University of Freiburg
[e] and University of Mining and Metallurgy, Cracow
[f] and Heisenberg Fellow
[g] now at Yale University, Dept of Physics, New Haven, USA
[h] and Depart of Experimental Physics, Lajos Kossuth University, Debrecen, Hungary.

tures a more sophisticated jet charge definition. Finally, it combines the single lepton and dilepton data.

2 Event selection

The analysis was performed on data collected by the OPAL detector at LEP in the vicinity of the Z^0 peak from 1991 to 1995. The OPAL detector has been described elsewhere [8,9]. Tracking of charged particles is performed by a central detector, consisting of a silicon microvertex detector, a vertex chamber, a jet chamber and z-chambers.[1] The central detector is positioned inside a solenoid, which provides a uniform magnetic field of 0.435 T. The silicon microvertex detector consists of two layers of silicon strip detectors; the inner layer covers a polar angle range of $|\cos\theta| < 0.83$ and the outer layer covers $|\cos\theta| < 0.77$. This detector provided measurements of hits in the r-ϕ plane for data taken since 1991, with z coordinates also measured since 1993. The vertex chamber is a precision drift chamber which covers the range $|\cos\theta| < 0.95$. The jet chamber is a large-volume drift chamber, 4.0 m long and 3.7 m in diameter, providing both tracking and ionisation energy loss (dE/dx) information. The z-chambers measure the z-coordinate of tracks as they leave the jet chamber in the range $|\cos\theta| < 0.72$. The coil is surrounded by a time-of-flight counter array and a barrel lead-glass electromagnetic calorimeter with a presampler. Including the endcap electromagnetic calorimeters, the lead-glass blocks cover the range $|\cos\theta| < 0.98$. The magnet return yoke is instrumented with streamer tubes and serves as a hadron calorimeter. Outside the hadron calorimeter are muon chambers, which cover 93% of the full solid angle.

Hadronic Z^0 decays were selected using criteria described in a previous publication [10]. Only data where the silicon microvertex detector was fully functional were accepted, resulting in 2.9 million hadronic Z^0 decays with 3-dimensional silicon readout (3D), and 0.9 million with silicon readout only in the r-ϕ projection (2D). Tracks and electromagnetic clusters not associated to tracks were grouped into jets using a cone jet algorithm [11].

The selection of electrons and muons as candidates for semileptonic decays of b hadrons followed the procedure described in the previous paper [4], the exception being that an improved purity tag at a later stage of the analysis allowed the cut on the lepton neural network $\alpha_{\rm kin}$ to be loosened from 0.7 to 0.5.

Monte Carlo events were generated using the Jetset 7.4 program [12] with parameters tuned to OPAL data [13], and were processed by the detector simulation program [14].

[1] The coordinate system is defined with positive z along the e^- beam direction, θ and ϕ being the polar and azimuthal angles. The origin is taken to be the centre of the detector and r is the distance to the z-axis

2.1 Proper time reconstruction

An attempt to reconstruct the proper decay time of the parent b hadron was made for each jet containing a lepton with a minimum p_t of 0.7 GeV/c relative to the jet axis. The algorithm used to reconstruct the decay length of the supposed parent b-hadron was different from that described previously [4]. In principle, each b jet should contain two vertices other than the primary vertex, corresponding to the decays of the b and c hadrons. These two vertices are referred to as the secondary and tertiary vertices, respectively. In the new algorithm, the positions of the secondary and tertiary vertices are allowed to vary independently in a maximum likelihood fit, where the likelihood is calculated for each vertex position by taking the product of likelihoods of all the tracks in the jet.

Each track contributes a likelihood of $(w/2) \times (P_s + P_t) + (1 - w) \times P_p$, where w is the probability for the track to originate from the secondary or tertiary vertex, as determined from the track momentum and angle relative to the jet direction. For the lepton candidate, w is fixed to 1. The quantities P_p, P_s and P_t are the probabilities for the track to be compatible with belonging to the primary, secondary or tertiary vertices respectively, based on the impact parameters relative to the assumed vertex positions both in r-ϕ and r-z.

Such a fit has 6 free parameters: the B decay length, the D decay length and two angles each for the B direction and the D direction. In practice, the power of the fit to measure the D decay length was found to be poor. The resolution was therefore improved by imposing a constraint on the D decay length, L_D: the likelihood was multiplied by $\exp(-L_D/L)$ where $L = 0.093$ cm was an average D decay length in the Monte Carlo, and L_D was constrained to be positive. The effect of this constraint is to put the fitted D decay length to 0 for most vertices, effectively reducing the number of free parameters to three. Gaussian constraints are imposed on the B direction angles, using the results of a B direction-finding algorithm similar to that described in [15], which weighted tracks according to their rapidity relative to the estimated B direction. Loose constraints were also imposed on the D direction angles. The B decay length was constrained[2] to lie in the range -0.4 cm to 2.5 cm.

For leptons coming from semileptonic B decays, according to Monte Carlo with 3D silicon information, about 4% of the jets considered were rejected as containing fewer than 3 tracks passing the quality requirements. In about 8% of cases the fit did not successfully converge, and these candidates were rejected. About 2% of the candidates were rejected with the fitted B decay length less than -0.4 cm. To ensure that the results of the fit were stable and unambiguous, candidates were rejected if the likelihood was improved when the decay length was increased by 1 standard deviation. In addition, a scan of the likelihood was made as a function of the B decay length with the other

[2] The constraint was implemented by subtracting a smooth penalty function from the log likelihood, which was 0 in the quoted range and parabolic outside this range

parameters kept fixed. If the log likelihood was within 1.75 of the fitted result for any B decay length further than two standard deviations from the central value, the candidate was rejected. These two requirements rejected about 24% of the candidates. Thus, in total, about 62% of leptons from B decays were selected with a successful fit. For these leptons, the B decay length, $L_{\rm B}$, and its uncertainty, σ_L, were taken directly from the fit.

Given a reconstructed secondary vertex, the B energy was determined in a similar way to that described previously [4,16]. The energy of the jet containing the lepton was reconstructed using the Z^0 mass to constrain the event kinematics, and the estimated contribution from fragmentation particles was subtracted. The fragmentation particles were separated from the b-hadron decay products using momentum, angle and vertex information. The uncertainty of the B boost, $\sigma_{\beta\gamma}$, was determined from the estimated uncertainties on the charged and neutral fragmentation energies, which were determined from the estimated probabilities for each track or cluster to originate from a fragmentation particle.

The selected vertices were split into two classes, A and B, according to the quality of the proper time reconstruction. The better quality secondary vertices (class A) were selected by requiring that

- the mass of the reconstructed vertex, using association probabilities for each track as calculated in the likelihood, was larger than 0.5 GeV;
- the χ^2 per degree of freedom of the vertex configuration was less than 6;
- the angle between the lepton direction and the vector joining the primary and secondary vertices was larger than 110 mrad;
- the ratio of lepton p_t (relative to the jet axis) and momentum p was less then 0.35;
- the reconstructed jet energy was required to not exceed the constrained jet energy by more than 2 GeV. The reconstructed jet energy, computed as the sum of energies of all tracks and clusters in the jet, should normally be smaller than the constrained jet energy because of the missing neutrino from the semileptonic decay.

Class A contains 67% of the selected vertices for leptons from B decays in Monte Carlo; the remaining 33% constitute class B.

The proper time, t, is given by [3]:

$$t = \frac{L_{\rm B}}{\beta\gamma} = \frac{m_{\rm B}}{\sqrt{E_{\rm B}^2 - m_{\rm B}^2}} L_{\rm B} \; . \tag{2}$$

As in the previous analysis [4], use is also made of the estimated uncertainty, σ_t, on the proper time, calculated from the separately estimated uncertainties on the decay length, σ_L, and the boost factor, $\sigma_{\beta\gamma}$:

$$\left(\frac{\sigma_t}{t}\right)^2 = \left(\frac{\sigma_L}{L_{\rm B}}\right)^2 + \left(\frac{\sigma_{\beta\gamma}}{\beta\gamma}\right)^2 \; , \tag{3}$$

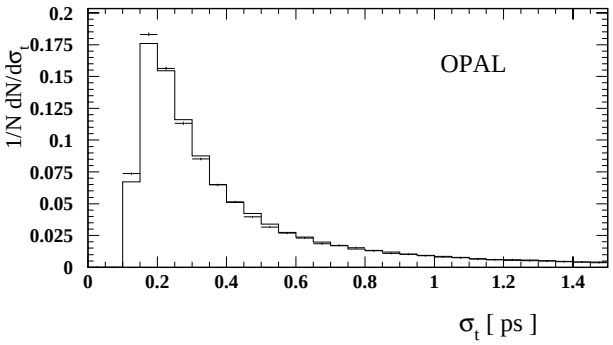

Fig. 1. The distribution of σ_t for all selected vertices in the data (points), together with the Monte Carlo prediction (histogram). The vertical error bars are obscured by the size of the points

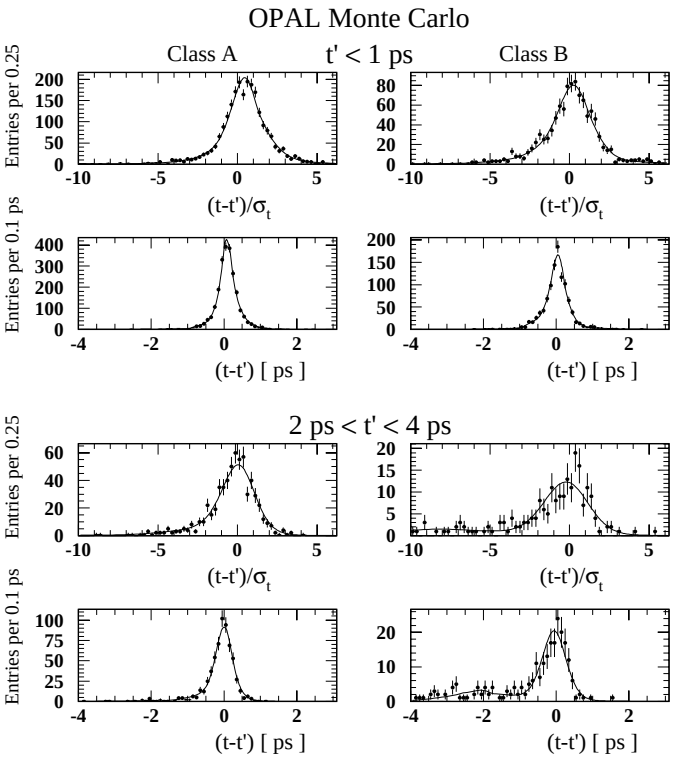

Fig. 2. The proper time resolution for Monte Carlo B_s^0 vertices with estimated $\sigma_t < 0.3$ ps separated into the two vertex classes, A and B, for two ranges of true proper time t'. The curves indicate the fitted resolution functions

where correlations between the uncertainties on $L_{\rm B}$ and $\beta\gamma$ are neglected. This is unimportant because the shape of the t distribution is parametrised from Monte Carlo, where such correlations are included. The distribution of estimated σ_t is shown for the data for all selected vertices in Fig. 1 together with the Monte Carlo prediction. The slight discrepancy that is visible is not important, as the analysis uses the value of σ_t estimated for each event. Plots indicating the proper time resolution for B_s^0 vertices with estimated $\sigma_t < 0.3$ ps are shown in Fig. 2, together with curves from the fitted resolution functions, defined

[3] We use the notation $\hbar = c = 1$

as in the previous paper [4]. Note that different resolution functions are used for class A and class B vertices. The plots are for the 3D silicon readout; the resolution functions were determined separately for events with 2D silicon readout, where the resolution is similar (though the efficiency is worse).

Events were accepted only if they contained at least one vertex with $\sigma_t < 0.3$ ps. This proper time resolution is necessary to give sensitivity to $\Delta m_s > 5\ \mathrm{ps}^{-1}$. A second identified lepton was considered only if separated by more than 60° from the first lepton (the leptons are ordered using p and p_t), to ensure that the leptons do not originate from the same b hadron. A second vertex in the event, containing a second identified lepton, was accepted if it had $\sigma_t < 0.6$ ps. These requirements led to 43598 events selected in the 3D data, of which 5012 had a second identified lepton and 1788 had two valid vertices. For the 2D data, 9452 events were selected, of which 1019 had a second identified lepton and 175 had two valid vertices. The distributions of reconstructed proper time are shown in Fig. 3 for the single lepton and dilepton events together with the Monte Carlo prediction. Only one proper time per event, satisfying $\sigma_t < 0.3$ ps, is included in the figure for the dilepton events. The proper time distributions are given separately for the 93-95 data and the 91-92 data (only 2D silicon information available). In both cases, the Monte Carlo gives a reasonable description of the data. Also indicated are the contributions from $b \to \ell$ decays and from hadronic Z^0 decays to $u\bar{u}$, $d\bar{d}$, $s\bar{s}$ or $c\bar{c}$. The remaining contributions from $b\bar{b}$ events, such as $b \to c \to \ell$ decays and background leptons, are not indicated, but are included in the total.

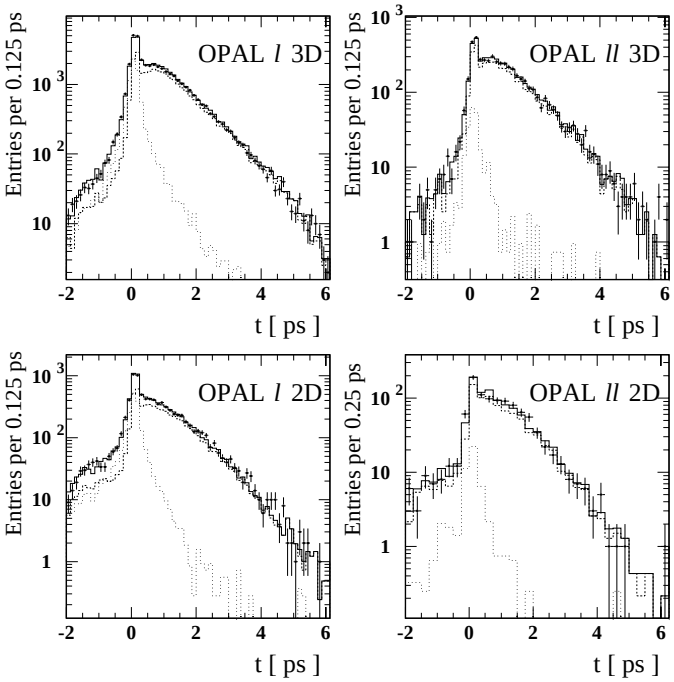

Fig. 3. The proper time distributions for vertices with $\sigma_t < 0.3$ ps for single and dilepton events with 3D and 2D silicon information available (points). The Monte Carlo predictions are superimposed (solid histograms), together with the contributions from $b \to \ell$ decays (dashed) and from $u\bar{u}$, $d\bar{d}$, $s\bar{s}$ or $c\bar{c}$ events (dotted)

3 Flavour tag

In order to detect oscillation, one needs to determine the b-flavour (b or $\bar{b}$) of the B_s^0 both at the time of production and decay. The flavour at decay is inferred from the charge of the daughter lepton. The flavour at production is obtained from the charge of a lepton, where available, in the hemisphere opposite to the first lepton. For events containing only one identified lepton, it is determined by a modified jet charge technique using information in both hemispheres. The rest of this section describes the modified jet charge technique.

3.1 Lepton hemisphere

The lepton hemisphere is defined by the axis of the jet that contains the lepton. For this hemisphere, an unweighted jet charge, as used in the previous analysis [4], has the desirable property that the decay products of a neutral B meson contribute a net charge of zero, provided they are fully contained in the jet. The jet charge therefore depends only on the net charge of the fragmentation tracks, and hence depends on the produced b-flavour. However, there is extra information that this method does not utilise. The leading charged meson from fragmentation should reflect the b production flavour; also, it should have a different angular distribution and a different momentum spectrum than the other fragmentation products. For B_s^0 production, this leading fragmentation meson should have an enhanced probability to be a K meson.

To exploit this supplementary information, a number of jet/hemisphere charge variables were defined:

- the unweighted jet charge, $\sum_i Q_i$, summing over all tracks in the jet;
- the unweighted hemisphere charge, $\sum_i Q_i$, summing over all tracks in the lepton hemisphere;
- $Q_{\mathrm{hem}}^{\mathrm{NN}}$, a weighted hemisphere charge, where a neural network is used to assign the weights (see below);
- $Q_{\mathrm{hem}}^{\mathrm{NN}\prime}$, a variant on $Q_{\mathrm{hem}}^{\mathrm{NN}}$ (see below).

Each of these variables was multiplied by the lepton charge, Q_ℓ, to provide sensitivity to mixing, and fed into a neural network, trained to separate unmixed B_s^0 decays (where the flavour is the same at production and decay) from mixed B_s^0 decays, with an output Q_{same} ('same' stands for the same hemisphere as the lepton).

To determine the weights used for $Q_{\mathrm{hem}}^{\mathrm{net}}$, a neural network was trained on B_s^0 hemispheres to distinguish fragmentation tracks whose charge is opposite to that of the produced b quark (as expected for the leading charged fragmention meson) from those that have the same charge. Four inputs were chosen per track: the rapidity relative to the jet, the track momentum divided by the jet energy and dE/dx weights for the π and K hypotheses. B decay products were excluded from the network training. The

neural network output, δ, gives a weak separation between right and wrong sign fragmentation tracks. A hemisphere charge was formed to exploit this:

$$Q_{\rm hem}^{\rm NN} = \sum_i Q_i \times (\delta_i - 0.5) \qquad (4)$$

where the summation is over all tracks in the same hemisphere as the lepton. However, the output range with the best separation also includes a large background from B_s^0 decay products. A second neural network, with output ϵ, was therefore implemented to separate fragmentation tracks from B decay products using the track impact parameters and significances in both r-ϕ and r-z projections. A variant on the above hemisphere charge was formed:

$$Q_{\rm hem}^{\rm NN\prime} = \sum_i Q_i \times (\delta_i - 0.5) \times \epsilon_i \qquad (5)$$

where the summation is over all tracks in the same hemisphere as the lepton.

This hemisphere charge is not optimal, because the important charge correlations between tracks (especially those from the B_s^0 decay) have been neglected. In fact, when combined with the lepton charge, the unweighted hemisphere or jet charge gives a separation of mixed and unmixed B_s^0 decays that is superior to that obtained with $Q_{\rm hem}^{\rm NN}$ or $Q_{\rm hem}^{\rm NN\prime}$. However, the correlation of $Q_{\rm hem}^{\rm NN(\prime)}$ with the unweighted hemisphere charge is not very strong, allowing the combination to achieve a superior performance.

The neural network output for the combination, $Q_{\rm same}$, is shown in Fig. 4a for unmixed and mixed B_s^0 decays. The power to separate mixed from unmixed B_s^0 decays is approximately 40% better than the unweighted hemisphere or the unweighted jet charge alone. The distribution of $Q_{\rm same}$ for the selected data events is compared to Monte Carlo in Fig. 5a, where a reasonable agreement is seen.

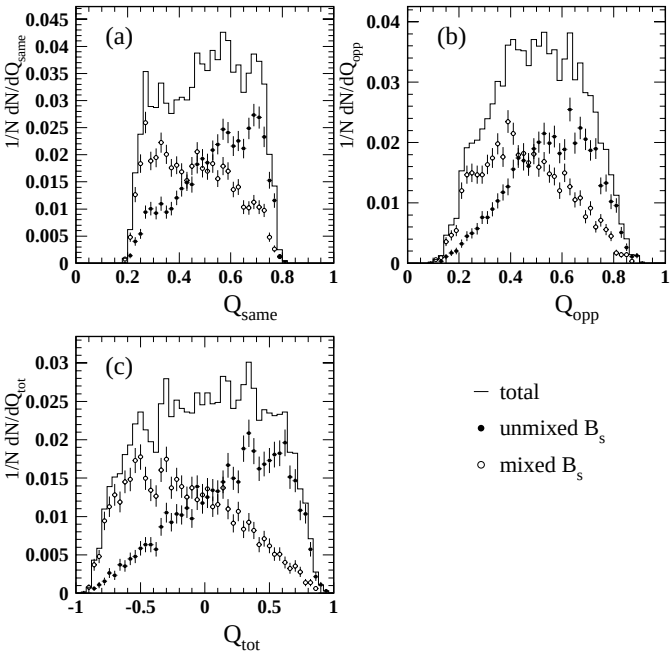

Fig. 4a–c. The distribution of **a** $Q_{\rm same}$, **b** $Q_{\rm opp}$ and **c** $Q_{\rm tot}$ for selected Monte Carlo events where the lepton originates from a B_s^0 decay. The components from unmixed and mixed B_s^0 decays are indicated

3.2 Opposite hemisphere

The opposite hemisphere is defined by the axis of the highest energy jet in the event other than the lepton jet. For this hemisphere, a similar approach was taken, though the situation is simpler in that it is not necessary to distinguish fragmentation particles from B decay products since both may carry useful charge information. A number of variables sensitive to the b production flavour were defined:

- $Q_{\rm jet} = \sum_i Q_i \left(\frac{p_i^l}{E_{\rm beam}}\right)^\kappa$ where the sum is over all tracks in the highest energy jet in the hemisphere using $\kappa = 1$ and p_i^l is the longitudinal momentum of track i relative to the jet axis;
- $Q_{\rm jet}$ using $\kappa = 0$;
- $Q_{\rm prob}$ defined below, using a neural network output for each track in the hemisphere opposite the lepton;
- vertex charge information - 2 parameters $Q_{\rm vtx}$ and σ_Q (see below).

The charge variables were multiplied by the lepton charge and a neural network, trained to separate unmixed B_s^0 decays from mixed B_s^0 decays, was used to combine the 5 input variables, giving an output $Q_{\rm opp}$.

For the $Q_{\rm prob}$ variable, a neural network was trained to enhance tracks with the desired charge correlation with the lepton (opposite in the absence of mixing), using the same four inputs per track as for the track neural network used in the lepton hemisphere. A probability ϱ that the lepton parent was produced as a $\bar{B}_s^0$ rather than a B_s^0 is formed for each track, i :

$$\varrho_i = Q_i \times (\zeta_i - 0.5) + 0.5 \,, \qquad (6)$$

where ζ_i is the output of this neural network for track i. The tracks are combined into an overall probability per hemisphere, assuming that the probabilities are independent :

$$Q_{\rm prob} = \frac{2 \times \prod_i \varrho_i}{\prod_i \varrho_i + \prod_i (1 - \varrho_i)} \,. \qquad (7)$$

The power of $Q_{\rm prob}$ to separate mixed from unmixed B decays, when multiplied by the lepton charge, is very similar to that of the conventional $Q_{\rm jet}^{\kappa=1}$ which was used in the previous paper [4]. The two quantities are strongly correlated, but some gain can still be achieved by combining them. Excluding the vertex charge information, the neural net combination of the 3 charge variables results in a hemisphere charge with a separation power 23% better than that of $Q_{\rm jet}^{\kappa=1}$ alone.

Further improvement to the opposite hemisphere charge tag can be made by tagging charged B decays using vertex charge, as described in a recent paper [17]. This

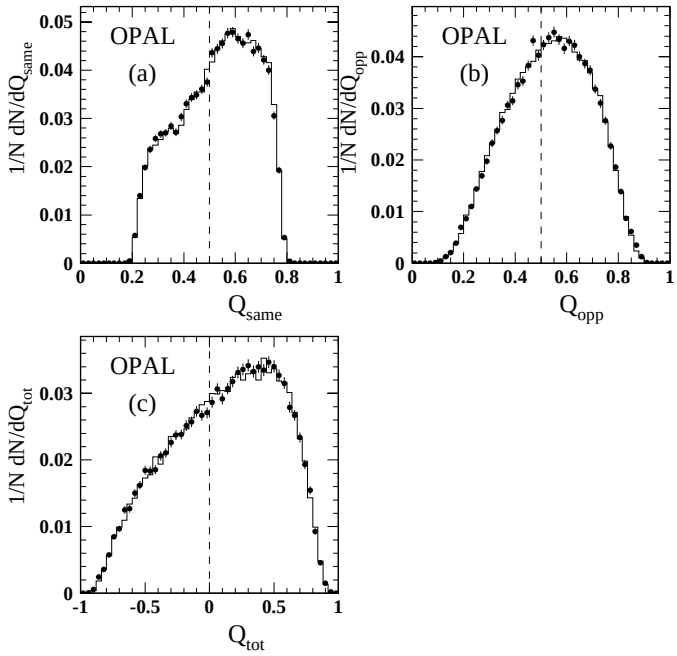

Fig. 5a–c. The distribution of **a** $Q_{\rm same}$, **b** $Q_{\rm opp}$ and **c** $Q_{\rm tot}$ for selected lepton events in the data (points) together with the Monte Carlo prediction (histogram). The dashed line marks the value of the charge variable where there is no information on the b production flavour

gave two variables: $Q_{\rm vtx}$ and σ_Q, which were available for about 40% of events (where vertices significantly separated from the primary vertex were found). This information, suitably transformed, was fed into the 5 input neural network. The 5 inputs were still used when no vertex information was available, with the extra 2 inputs set to register the lack of information. A further improvement of about 10% in separation power was obtained from the inclusion of the vertex charge information, and the network output, $Q_{\rm opp}$, is shown in Fig. 4b for unmixed and mixed B_s^0 decays. The distribution of $Q_{\rm opp}$ for the selected data events, shown in Fig. 5b, is well described by the Monte Carlo prediction.

3.3 Combined flavour tag

The Monte Carlo test samples indicate that the individual values of both $Q_{\rm same}$ and $Q_{\rm opp}$ give the charge tag purity for B_s^0 mesons fairly accurately. Since they are largely independent they may be combined simply to give a measure of the probability that the B_s^0 mixed:

$$Q_{\rm tot} = \frac{Q_{\rm same} \times Q_{\rm opp} \times 2}{Q_{\rm same} \times Q_{\rm opp} + (1 - Q_{\rm same})(1 - Q_{\rm opp})} - 1 \ , \quad (8)$$

where the offset of -1 is introduced so that when $Q_{\rm tot} = 0$ there is no information on whether the B_s^0 mixed. The performance of $Q_{\rm tot}$ is shown in Fig. 4c, and has a separation power that is 40% better than $Q_{\rm 2jet}$, used in the previous analysis [4]. The distribution of $Q_{\rm tot}$ for the selected data events is shown in Fig. 5, together with the Monte Carlo prediction. The good agreement observed serves as a check on the power of the charge tag.

4 Determination of the b purity

The selected lepton candidates contain significant contributions from sources other than the semileptonic decays of b hadrons, notably $b \to c \to \ell$ decays, background leptons either in $Z \to b\bar{b}$ events or in lighter quark events and $c \to \ell$ decays in $Z \to c\bar{c}$ events [4]. The probability that a lepton candidate originated from a given source, ignoring lifetime information in the lepton jet, was evaluated using properties of the lepton jet and of the opposite hemisphere. These probabilities are used in the fit (described later) to scale the likelihood functions corresponding to each source, where these likelihood functions describe the reconstructed proper time and charge correlation.

For single lepton events, the value of $\alpha_{\rm kin}$, the lepton neural network output, was used together with a b-tag from the opposite hemisphere to produce a single variable that measures the purity of semileptonic decays of b hadrons. For dilepton events the purity was determined from the two values of $\alpha_{\rm kin}$.

The opposite hemisphere tag selects the highest energy jet in the thrust hemisphere opposite to that containing the lepton jet. In this jet, a neural network was used to separate tracks with good quality 3D impact parameter information coming from b jets from those coming from light quark jets (u, d or s). The inputs were the impact parameters and their significances in both projections, the distance of closest approach of the track to the jet axis and the χ^2 for the track to intersect this axis. The neural network outputs for the individual tracks were multiplied together to form a jet probability, $p_{j3\rm D}$. Not all tracks with silicon information in the r-ϕ plane have reliable 3D impact parameter information, so a simpler variable was also constructed, based solely on the impact parameter significances in the r-ϕ plane. In this case, $p_{j2\rm D}$ was constructed by multiplying the likelihoods for each track to be consistent with the primary vertex. The likelihood had a simple double-Gaussian form. A neural network combined $p_{j3\rm D}$, $p_{j2\rm D}$, the numbers of tracks used for each of these quantities, the $|\cos\theta|$ of the jet axis, and Fox-Wolfram moments which also have distinguishing power between b jets and light-quark jets. The neural network was trained to separate b jets from u, d or s jets (charm events have properties that are intermediate). The neural network output, $\beta_{\rm hemi}$, is shown in Fig. 6 for $b\bar{b}$ events and events from lighter quarks.

To form the event b-tag $\beta_{\rm evt}$, a neural network was used to combine $\alpha_{\rm kin}$ with $\beta_{\rm hemi}$ (though simply multiplying together the purities obtained from each tag would yield a similar performance). The distribution of $\beta_{\rm evt}$ is shown in Fig. 7 for the data, together with the Monte Carlo prediction and the component from semileptonic decays of b hadrons. Also shown in the figure are the corresponding $\beta_{\rm evt}$ distributions with $t > 1$ ps. A comparison of these two figures indicates that the light quark background is reasonably modelled.

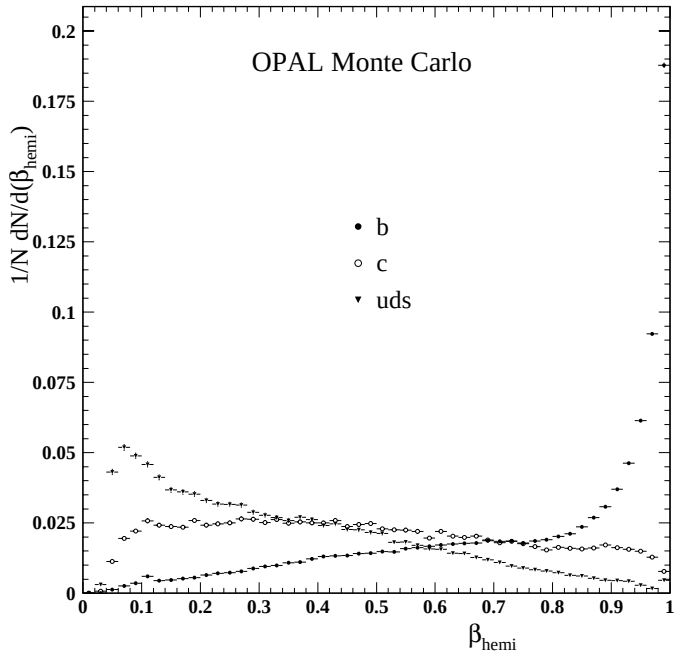

Fig. 6. Distribution of $\beta_{\rm hemi}$ in $b\overline{b}$ events, $c\overline{c}$ events and light quark events

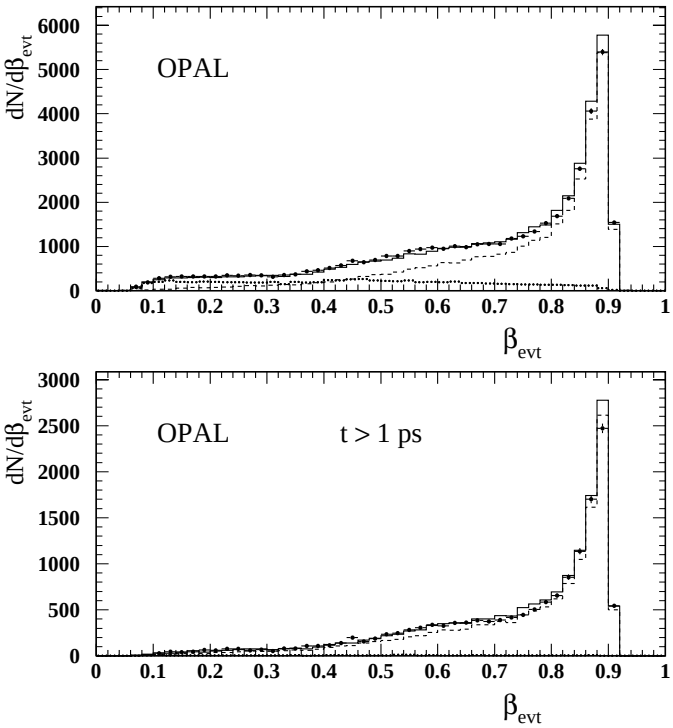

Fig. 7. The upper plot shows the distribution of $\beta_{\rm evt}$ for the data (points) together with the Monte Carlo prediction (solid line). The lower plot shows the same thing but with a minimum reconstructed proper time of 1 ps. The components from the semileptonic decays of b hadrons (dashed line) and from $u\overline{u}$, $d\overline{d}$, $s\overline{s}$ or $c\overline{c}$ (dotted line) are also indicated. The latter component is almost invisible in the lower plot

5 Fit for $\Delta m_{\rm s}$

A maximum likelihood fit was constructed, similar to that described previously for single lepton events [4] and for dilepton events [16]. The following quantities were input per event for the three classes of events :

1. single lepton events : t, σ_t, $Q_{\rm tot}$ and $\beta_{\rm evt}$;
2. dilepton events with one vertex : t, σ_t, $Q_\ell^{(1)} \cdot Q_\ell^{(2)}$, $\alpha_{\rm kin}^{(1)}$ and $\alpha_{\rm kin}^{(2)}$;
3. dilepton events with two vertices : $t^{(1)}$, $\sigma_t^{(1)}$, $t^{(2)}$, $\sigma_t^{(2)}$, $Q_\ell^{(1)} \cdot Q_\ell^{(2)}$, $\alpha_{\rm kin}^{(1)}$ and $\alpha_{\rm kin}^{(2)}$,

where the superscripts are used to differentiate between the two leptons where appropriate. As mentioned before, the purities of the different sources were calculated event-by-event from the appropriate inputs, taking the distributions of these quantities from Monte Carlo for each source.

The Monte Carlo predicts that $b\overline{b}$ events account for 81% of the single lepton events, 93.6% of the dilepton events with one vertex and 98.3% of the dilepton events with two vertices. For the selected vertices in $b\overline{b}$ events, 87.5% were predicted to come from $b \to \ell$ (or $b \to \bar{c} \to \ell$, $b \to \tau \to \ell$, or $b \to J/\psi \to \ell$) [4] decays and 9.2% from $b \to c \to \ell$ (or $b \to J/\psi \to \ell$) decays. Of the $b \to \ell$ decays, an estimated 10.5% involve B_s^0 mesons.

In this paper, the only parameter that is varied in the fit is the B_s^0 oscillation amplitude, A, as defined in [18] and used in the previous paper [4]. The probability density for a produced B_s^0 to decay as a B_s^0 after time t' is:

$$\mathcal{P}_{\rm unmix} = \frac{\exp(-\frac{t'}{\tau})}{\tau} \cdot \frac{1 + A\cos\Delta m_{\rm s} t'}{2}$$

and to decay as a $\bar{B}_s^0$ is :

$$\mathcal{P}_{\rm mix} = \frac{\exp(-\frac{t'}{\tau})}{\tau} \cdot \frac{1 - A\cos\Delta m_{\rm s} t'}{2} \ ,$$

where τ is the B_s^0 lifetime. At the true oscillation frequency, the fitted value of A should be consistent with 1. Far from the true frequency, the expectation value for A is 0. Therefore, values of $\Delta m_{\rm s}$ may be excluded when A is below 1 and inconsistent with 1. Since $\Delta m_{\rm s}$ is large, the fitted value of A is relatively insensitive to sources of systematic uncertainty that affect the mean $Q_{\rm tot}$ or the overall like-sign fraction in the case of the dilepton events. Therefore a complicated fitting scheme, as used in the previous paper [4], to reduce the impact of these systematic errors is not necessary here. This also implies that this analysis is not optimal for $\Delta m_{\rm s}$ values below about 2 ps^{-1}.

Unlike the previous analysis [4], the purity of the b production flavour tag is taken to be independent of $\Delta m_{\rm s}$ or the fitted amplitude. The uncertainty on this tagging purity is assessed from the comparison of data and Monte Carlo shown in Fig. 5. This agreement is also sensitive to

[4] The decays $b \to \bar{c} \to \ell$, $b \to \tau \to \ell$ and half of the $b \to J/\psi \to \ell^+\ell^-$ decays are classed together with $b \to \ell$ because they have the same charge correlation between the lepton and the b quark

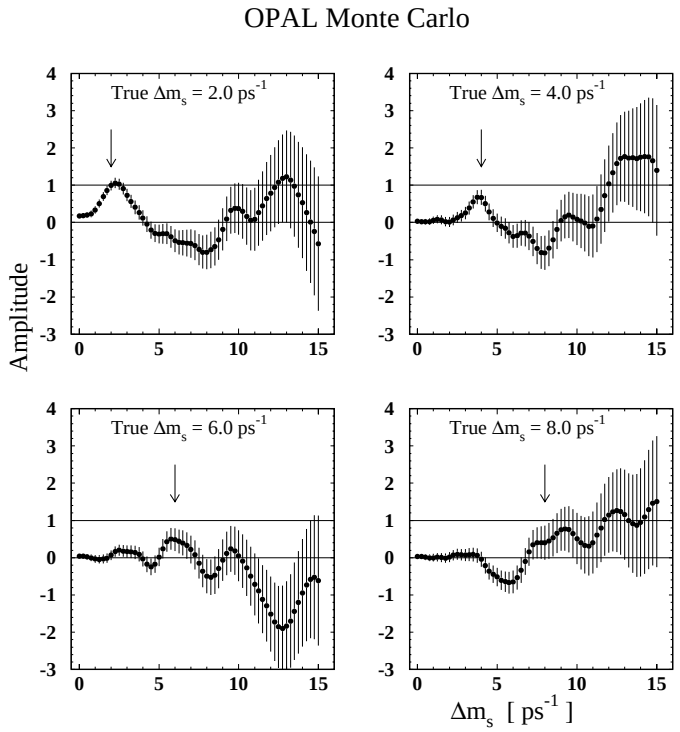

Fig. 8. The fitted value of A as a function of Δm_s for Monte Carlo data sets simulated using four different Δm_s values. The four data sets are statistically correlated

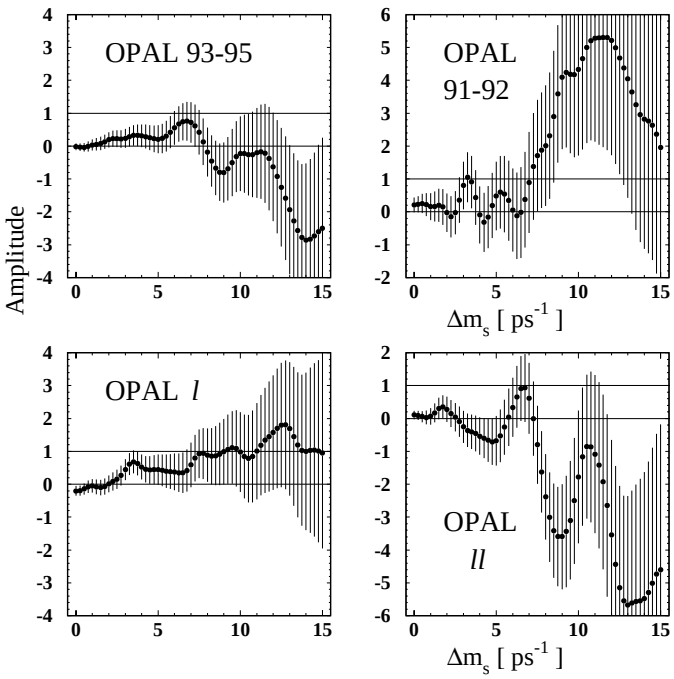

Fig. 9. The fitted amplitude as a function of Δm_s for the data collected from 93 to 95 (3D silicon) and that collected in 91 and 92 (2D silicon), and for single lepton and dilepton data (where the $91-92$ and $93-95$ data are combined). The errors are statistical

the overall mixed fraction, χ, averaged over all b hadrons - which is measured to be 0.118 ± 0.006 [1] and the fraction of $b \to c \to \ell$ decays, taken to have a 15% uncertainty [4].

6 Results

The performance of the fit was first tested using Monte Carlo simulated data. Figure 8 shows the fitted amplitude as a function of Δm_s for four samples generated with different true Δm_s values. These four Monte Carlo samples are statistically correlated, because the same Monte Carlo events are used to simulate different oscillation frequencies. Each represents 6.8 million hadronic Z decays (approximately double the statistics available in the data). The behaviour of these samples is consistent with expectation. At low values of true Δm_s, a clear peak is seen at $A = 1$, while at higher frequencies the sensitivity is insufficient. In addition, tests were performed for true Δm_s values up to 15 ps^{-1} using additional Monte Carlo samples containing only $Z \to b\bar{b}$ events. The results of these tests, representing greater statistical power, were also consistent with expectation.

For the data, separate results were obtained for the 91-92 data (2D silicon) (9452 events selected) and the 93-95 data (3D silicon) (43598 events selected). These results are shown in Fig. 9, where the errors are statistical only. The data can also be split into single lepton (47109 events) and dilepton (6031 events) samples. These results are also shown in Fig. 9. It can be seen that the single lepton results are more precise, except at very low frequency, where the dilepton events are sensitive to mixing on both sides of the event. No significant evidence for a signal at any particular frequency is seen in any of the four plots. The fact that the measured amplitude is consistent with 0 at low frequencies, in each case, implies that no systematic problems are evident.

6.1 Systematic errors

Systematic errors arise from a number of sources. Their effect was determined by varying the appropriate parameter and obtaining a new set of amplitude results. This was done using the full data sample, with the exception of the resolution function uncertainties where Monte Carlo was also used, as described below.

The sources of systematic error considered are given in Table 1. In this table, f_s and f_{baryon} are the production fractions $f(b \to B_s^0)$ and $f(b \to b\ baryon)$. The $b \to c \to \ell$ parameter represents a single scaling factor for the fraction of events due to $b \to c \to \ell$ decays. The $Z \to c\bar{c}$ parameter represents a scale factor for the fraction of single lepton events due to $Z \to c\bar{c}$ decays. The effect is squared for the dilepton events. The lepton background number is a factor for the non-prompt background rate for each lepton. The quantity τ^+/τ_d represents the lifetime ratio for B^+ relative to B^0 mesons, and similarly for τ_s/τ_d and τ_{Λ_b}/τ_d. These ratios also affect the composition of the sample, as the semileptonic branching ratios of the individual b hadrons are taken to be proportional to the lifetimes. As mentioned in the introduction, the analysis is sensitive to B_d^0 as well

Table 1. Sources of systematic error

Parameter	Range
f_s	$10.5^{+1.8}_{-1.7}$% [1]
$f_{\rm baryon}$	$10.1^{+3.9}_{-3.1}$% [1]
$b \to c \to \ell$	±15% × nominal [4]
$Z \to c\bar{c}$	±20% × nominal [4]
Lepton background	±20% × nominal [4]
$\langle\tau_b\rangle$	1.564 ± 0.014 ps [1]
τ^+/τ_d	1.04 ± 0.04 [1]
τ_s/τ_d	0.99 ± 0.05 [1]
τ_{Λ_b}/τ_d	0.79 ± 0.05 [1]
Δm_d	0.464 ± 0.018 ps^{-1}[1]
Jet charge	±0.01 in tagging purity at $Q_{\rm tot} = 0.4$
Resolution function 1	worsen tracking resolution by 11%
Resolution function 2	shift $\langle x_E\rangle_b$ by 0.02

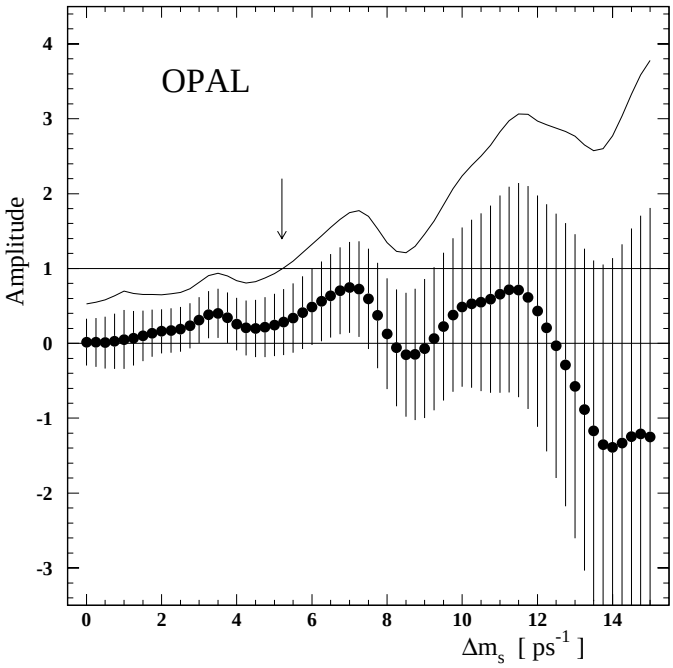

Fig. 10. Combined amplitude results for the entire data. The errors shown include both statistical and systematic errors. Also indicated is the 'limit' curve which is $A + 1.645\sigma_A$. All regions where this curve lies below $A = 1$ are excluded in method (a)

as B_s^0 oscillation, so a systematic uncertainty results from the value of Δm_d input.

The systematic error due to the tagging purity of the b production flavour as determined from jet charge was mentioned above. The error was modelled by changing the relative separation of the mixed and unmixed distributions of $Q_{\rm tot}$. The uncertainty on this offset was assessed using the comparison of the fraction of data with positive $Q_{\rm tot}$ as a function of $|Q_{\rm tot}|$ between data and Monte Carlo simulated events, taking into account uncertainties in the knowledge of χ and the fraction of $b \to c \to \ell$ decays. The table gives the size of the effect on the tagging purity at $Q_{\rm tot} = 0.4$ as an example.

The resolution functions are determined from Monte Carlo (see Fig. 2), and so are affected by uncertainties in the simulation of the data. Two such effects are considered: firstly, the resolution of d_0 and ϕ_0 was worsened for all tracks by 11%, where d_0 is the impact parameter relative to the primary vertex in the r-ϕ plane, and ϕ_0 is the ϕ angle at this point. This change represents the level of uncertainty in the tracking resolution. Secondly, the mean scaled energy of b hadrons, $\langle x_E\rangle_b$, was lowered by 0.02. Such a change represents a shift of over 2σ with respect to the measured value [19], but is inflated to include the effect of shape uncertainties in the b fragmentation function. Significant statistical fluctuations were observed in the estimated systematic errors due to the resolution functions. To reduce this effect, the systematic errors were estimated using a Monte Carlo sample together with the data, giving a total sample size equivalent to 10.6 million hadronic Z^0 decays. Uncertainty due to charm fragmentation is expected to have a negligible effect, and was neglected.

The individual systematic errors are given for the range of Δm_s values between 0 and 15 ps^{-1} in steps of 1 ps^{-1} in Table 2. The sign of the change in amplitude is indicated by $\pm$ or $\mp$ in each case, where $\pm$ indicates that A increases as the parameter in question increases. In the case of jet charge, the sign is defined relative to an increase in the charge tagging purity. For the resolution function uncertainty due to tracking resolution, the sign is defined relative to the change described above. The table also includes the overall fitted amplitude and its statistical error at these points. From the table it can be seen that the resolution function uncertainties dominate the systematic error at high frequencies, while the level of $b \to c \to \ell$ decays is important at low frequencies. The combined amplitude results for the 91-92 and 93-95 data together with the total errors are shown in Fig. 10.

6.2 Exclusion regions

To determine exclusion regions at 95% confidence level, we represent the measured value of A at a given value of Δm_s as a Gaussian distribution function $G(A - \mu, \sigma_A)$, where μ is the measured central value and σ_A is the measurement error. Two alternative methods are then considered to determine whether the value of Δm_s is excluded:

a) values are excluded where the probability of measuring an amplitude lower than that observed would be less than 5% were that value of Δm_s the correct one, i.e.

$$\int_1^\infty G(A - \mu, \sigma_A)\mathrm{d}A < 0.05\,, \qquad (9)$$

or

Table 2. Fit results for amplitude A, with the breakdown of systematic error contributions

Δm_s (ps^{-1})	0	1	2	3	4	5	6	7
A	.02	.05	.16	.31	.26	.25	.49	.75
σ_A^{stat}	±.09	±.16	±.22	±.27	±.32	±.39	±.48	±.57
f_s	±.13	±.16	±.07	±.02	±.02	±.01	∓.02	∓.05
f_{baryon}	∓.02	∓.01	∓.01	∓.01	∓.01	∓.01	∓.01	∓.01
$b \to c \to \ell$	±.20	±.24	±.10	±.04	±.02	±.00	∓.01	∓.01
$Z \to c\bar{c}$	∓.02	∓.04	∓.03	∓.03	∓.03	∓.03	∓.03	∓.02
Lepton background	±.05	±.09	±.10	±.11	±.11	±.12	±.13	±.15
$\langle\tau_b\rangle$	∓.00	∓.00	∓.00	∓.00	∓.00	∓.00	∓.00	∓.00
τ^+/τ_d	∓.05	∓.01	∓.01	∓.01	∓.01	∓.01	∓.01	∓.01
τ_s/τ_d	±.04	±.03	∓.00	∓.01	∓.01	∓.01	∓.01	∓.01
τ_{Λ_b}/τ_d	∓.01	∓.00	∓.00	∓.00	∓.00	∓.00	∓.00	∓.00
Δm_d	±.05	±.00	±.00	±.01	±.01	±.02	±.02	±.02
Jet charge	∓.14	∓.18	∓.10	∓.05	∓.04	∓.03	∓.06	∓.07
Tracking resolution	±.01	±.02	±.06	±.06	±.02	±.00	∓.10	∓.07
b fragmentation	±.00	±.00	±.05	±.04	±.08	±.05	∓.01	∓.07
σ_A^{syst}	±.30	±.36	±.20	±.15	±.15	±.14	±.18	±.20

Δm_s (ps^{-1})	8	9	10	11	12	13	14	15
A	.13	−.07	.48	.66	.43	−.57	−1.39	−1.25
σ_A^{stat}	±.69	±.85	±1.04	±1.25	±1.49	±1.73	±2.01	±2.34
f_s	±.04	±.08	±.03	±.01	±.07	±.25	±.39	±.41
f_{baryon}	∓.01	∓.01	∓.01	∓.01	∓.00	∓.00	∓.00	∓.01
$b \to c \to \ell$	∓.01	∓.01	±.02	±.02	±.02	±.05	±.07	±.12
$Z \to c\bar{c}$	∓.03	∓.04	∓.04	∓.04	∓.06	∓.09	∓.11	∓.13
Lepton background	±.15	±.16	±.21	±.25	±.29	±.33	±.37	±.44
$\langle\tau_b\rangle$	∓.00	∓.00	∓.00	∓.00	∓.00	∓.00	∓.00	±.01
τ^+/τ_d	∓.01	∓.02	∓.03	∓.03	∓.03	∓.03	∓.04	∓.06
τ_s/τ_d	∓.00	±.01	±.04	±.03	±.03	±.04	±.06	±.10
τ_{Λ_b}/τ_d	∓.00	∓.01	∓.01	∓.01	∓.01	∓.01	∓.01	∓.02
Δm_d	±.02	±.02	±.02	±.02	±.02	±.01	±.01	±.03
Jet charge	∓.01	±.02	∓.03	∓.05	∓.02	±.05	±.05	∓.01
Tracking resolution	∓.09	∓.08	∓.01	±.05	±.25	±0.97	±1.43	±1.59
b fragmentation	∓.19	∓.31	±.03	±0.32	±0.02	∓.14	∓.09	∓0.95
σ_A^{syst}	±.26	±.38	±.23	±.41	±.40	±1.07	±1.54	±1.96

b) the same definition, but limited to the positive region, i.e.

$$\frac{\int_1^\infty G(A-\mu,\sigma_A)\mathrm{d}A}{\int_0^\infty G(A-\mu,\sigma_A)\mathrm{d}A} < 0.05\,. \qquad (10)$$

The first definition gives a true 95% confidence level, in the sense that there is a 5% probability to exclude the true value. However, it is not protected against setting limits well beyond the experimental sensitivity. The second definition makes use of the fact that the predicted value of A cannot be less than 0, regardless of the value of Δm_s. It is automatically protected against setting limits beyond the sensitive range. For a true value of Δm_s well beyond the sensitive range, method (a) would exclude the true value in 5% of the experiments, while for method (b) this percentage would tend towards zero.

For method (a) the excluded regions may be determined simply by plotting the curve $A + 1.645\sigma_A$ as a function of Δm_s (Fig. 10). All regions where the curve lies below $A = 1$ may be excluded. This gives a lower limit $\Delta m_s > 5.2$ ps^{-1} at the 95% confidence level. The limit that would be obtained, were A measured to be 0 at every value of Δm_s, is 7.0 ps^{-1}. This is known as the sensitivity of the analysis.

For method (b), the confidence level must be calculated at each Δm_s point, according to the above formula.

This gives the result $\Delta m_s > 5.0$ ps^{-1} at the 95% confidence level, very similar to the method (a) result.

7 Conclusion

Single lepton and dilepton events were used to study B_s^0 oscillations with improved sensitivity with respect to previous OPAL papers [4,5]. The experiment was not able to resolve the oscillations, but can place a lower limit $\Delta m_s > 5.2$ ps^{-1} at the 95% confidence level. This result is consistent with previous publications [4–7], and supersedes the previously published OPAL results [4,5]. The sensitivity of the analysis (the lower limit that would be expected were the true oscillation frequency very large) was found to be 7.0 ps^{-1}, the second highest relative to previous publications [6,7].

Acknowledgements. We particularly wish to thank the SL Division for the efficient operation of the LEP accelerator at all energies and for their continuing close cooperation with our experimental group. We thank our colleagues from CEA, DAPNIA/SPP, CE-Saclay for their efforts over the years on the time-of-flight and trigger systems which we continue to use. In addition to the support staff at our own institutions we are pleased to acknowledge the Department of Energy, USA, National Science Foundation, USA, Particle Physics and Astronomy Research Council, UK, Natural Sciences and Engineering Research Council, Canada, Israel Science Foundation, administered by the Israel Academy of Science and Humanities, Minerva Gesellschaft, Benoziyo Center for High Energy Physics, Japanese Ministry of Education, Science and Culture (the Monbusho) and a grant under the Monbusho International Science Research Program, Japanese Society for the Promotion of Science (JSPS), German Israeli Bi-national Science Foundation (GIF), Bundesministerium für Bildung, Wissenschaft, Forschung und Technologie, Germany, National Research Council of Canada, Research Corporation, USA, Hungarian Foundation for Scientific Research, OTKA T-029328, T023793 and OTKA F-023259.

References

1. Particle Data Group, C. Caso *et al.*, Eur. Phys. J. **C 3** (1998) 1.
2. A. Ali and D. London, Z. Phys. **C 65** (1995) 431, and references therein.
3. Y. Nir, Phys. Lett. **B 327** (1994) 85.
4. OPAL Collaboration, K. Ackerstaff *et al.*, Z. Phys. **C 76** (1997) 401.
5. OPAL Collaboration, K. Ackerstaff *et al.*, Z. Phys. **C 76** (1997) 417.
6. ALEPH Collaboration, Eur. Phys. J. **C 7** (1999) 553; ALEPH Collaboration, Phys. Lett. **B 377** (1996) 205; ALEPH Collaboration, Eur. Phys. J. **C 2** (1998) 197.
7. DELPHI Collaboration, W. Adam *et al.*, Phys. Lett. **B 414** (1997) 382.
8. OPAL Collaboration, K. Ahmet *et al.*, Nucl. Instr. and Meth. **A 305** (1991) 275.
9. P.P. Allport *et al.*, Nucl. Instr. and Meth. **A 324** (1993) 34; P.P. Allport *et al.*, Nucl. Instr. and Meth. **A 346** (1994) 476.
10. OPAL Collaboration, G. Alexander *et al.*, Z. Phys. **C 52** (1991) 175.
11. OPAL Collaboration, R. Akers *et al.*, Z. Phys. **C 63** (1994) 197. The jet finding parameters ϵ and R were set to 5.0 GeV and 0.5, respectively.
12. T. Sjöstrand, Comp. Phys. Comm. **39** (1986) 347; M. Bengtsson and T. Sjöstrand, Comp. Phys. Comm. **43** (1987) 367; M. Bengtsson and T. Sjöstrand, Nucl. Phys. **B 289** (1987) 810; T. Sjöstrand, CERN-TH/6488-92.
13. OPAL Collaboration, G. Alexander *et al.*, Z. Phys. **C 69** (1996) 543.
14. J. Allison *et al.*, Nucl. Instr. and Meth. **A 317** (1992) 47.
15. OPAL Collaboration, K. Ackerstaff *et al.*, Z. Phys. **C 74** (1997) 413.
16. OPAL Collaboration, R. Akers *et al.*, Z. Phys. **C 66** (1995) 555.
17. OPAL Collaboration, K. Ackerstaff *et al.*, Eur. Phys. J. **C 5** (1998) 379.
18. H.G. Moser and A. Roussarie, Nucl. Instr. and Meth. **A 384** (1997) 491.
19. OPAL Collaboration, G. Alexander *et al.*, Phys. Lett. **B 364** (1995) 93; ALEPH Collaboration, D. Buskulic *et al.*, Phys. Lett. **B 357** (1995) 699.